Supplement of Geosci. Model Dev., 16, 5473–5492, 2023
https://doi.org/10.5194/gmd-16-5473-2023-supplement

Geoscientific Model Development
Open Access
EGU

Supplement of

Simulation of a fully coupled 3D glacial isostatic adjustment – ice sheet model for the Antarctic ice sheet over a glacial cycle

Caroline J. van Calcar et al.

Correspondence to: Caroline J. van Calcar (c.j.vancalcar@tudelft.nl)

Supplemental materials

Fig. S.1 shows the sea level and temperature forcing for the coupled model simulations. This forcing is in the results of previous simulations of de Boer et al. (2013) where ANICE was used to reconstruct global ice volume and the continental mean temperature at the northern hemisphere over the past 1 Myr. Those simulations used the LR04 benthic δ18O stack of 57 deep-sea sediment records as forcing (van de Wal., 2011). The results lead to a past surface-air temperature and eustatic sea level.

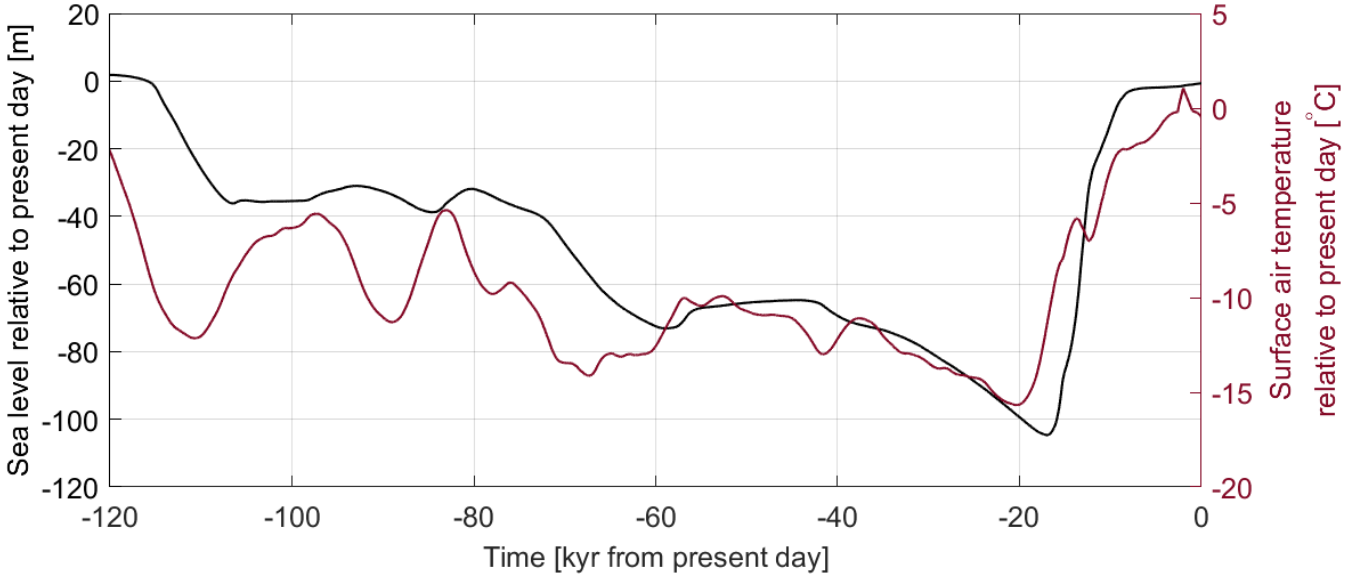

Figure S.1: Atmospheric temperature (black) and eustatic sea level relative to present-day (red). Both are shown over time, starting 120 kyears before present.

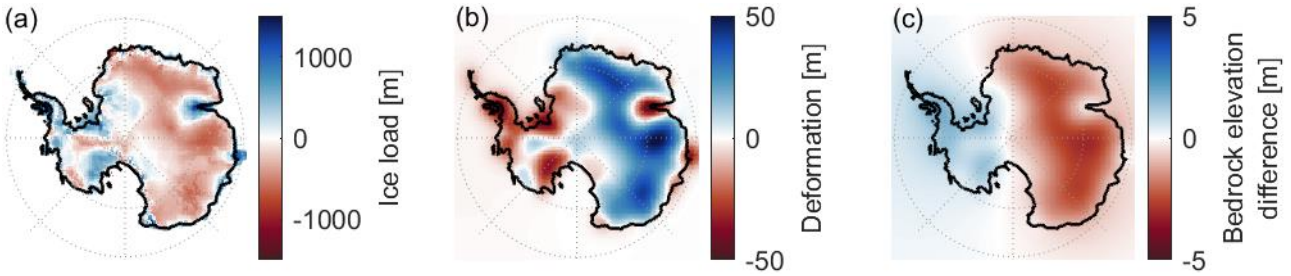

Figure S.2: Two simulations are performed using the 1D21 GIA model, one with the effect of self-gravity and one without the effect of self-gravity on bedrock deformation. The applied ice load is the change in ice load computed by ANICE using ELRA from 120 ka to 115 ka. Panel a shows the applied ice load over a period of 5000 yr. This change in ice load is the highest change simulated by the 1D21 coupled model over a glacial cycle. Panel b shows the resulting bedrock deformation when the effect of self-gravity is excluded. Panel c shows the bedrock elevation after 5000 yr when the effect of self-gravity is excluded subtracted from the bedrock elevation after 5000 yr when the effect of self-gravity is included.

Fig. S.3 shows the results of the tests performed to determine the resolution of the GIA model with the best trade-off between accuracy in deformation and the computation time. A 1D viscosity of 1020 Pa·s is used. The tests are performed using ice loading in the shape of a parabolic ice cap of 1500 meter thick with a radius of 1500 meter that is linearly applied to the GIA model over a time step of 1000 years. The near field resolution is varied between 15, 30, 55 and 70 km, shown on the horizontal axis, and the far field resolution is varied between 100 and 200 km, shown as dashed and solid lines respectively. For each test, we measured the computation time, shown on the left vertical axis, and we computed the maximum deformation of each simulation, shown on the right vertical axis. As expected, the dashed black line, referring to the runtime of the test with a far field resolution of 100 km, lies much higher than the solid black line, which refers to the runtime of the test with a far field resolution of 200 km. Following the red lines, the maximum difference in deformation with the coarsest resolution (70 km near field-200 km far field resolution) and the finest resolution is 11 cm (15 km near field-100 km far field resolution). However, the computation time is three times as long for the 30 km near field-100 km far field resolution compared to the 30 km near field-200 km far field resolution, while the difference with the higher resolution test is only 5 cm on a total deformation of 171 meter. Also, when considering far field resolution of 200 km, the near field resolution test of 15 km takes twice as long as the near field resolution test of 30 km whereas the difference in deformation is only 2 cm over 1000 years. We therefore chose a far field resolution of 200 km and a near field resolution of 30 km.

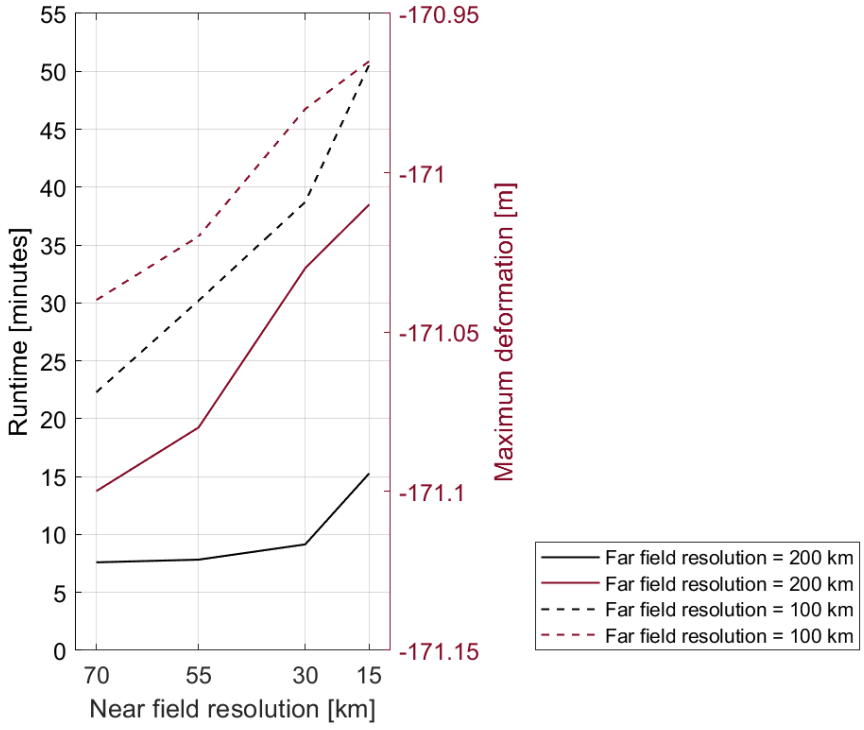

Figure S.3: The test simulations of 1000 years were conducted using a paraboloid ice load of 1500 meter thick. The x axis shows the near field resolution around Antarctica, the solid lines correspond to a far field resolution of 200 km and the dashed lines to a far field resolution of 100 km.

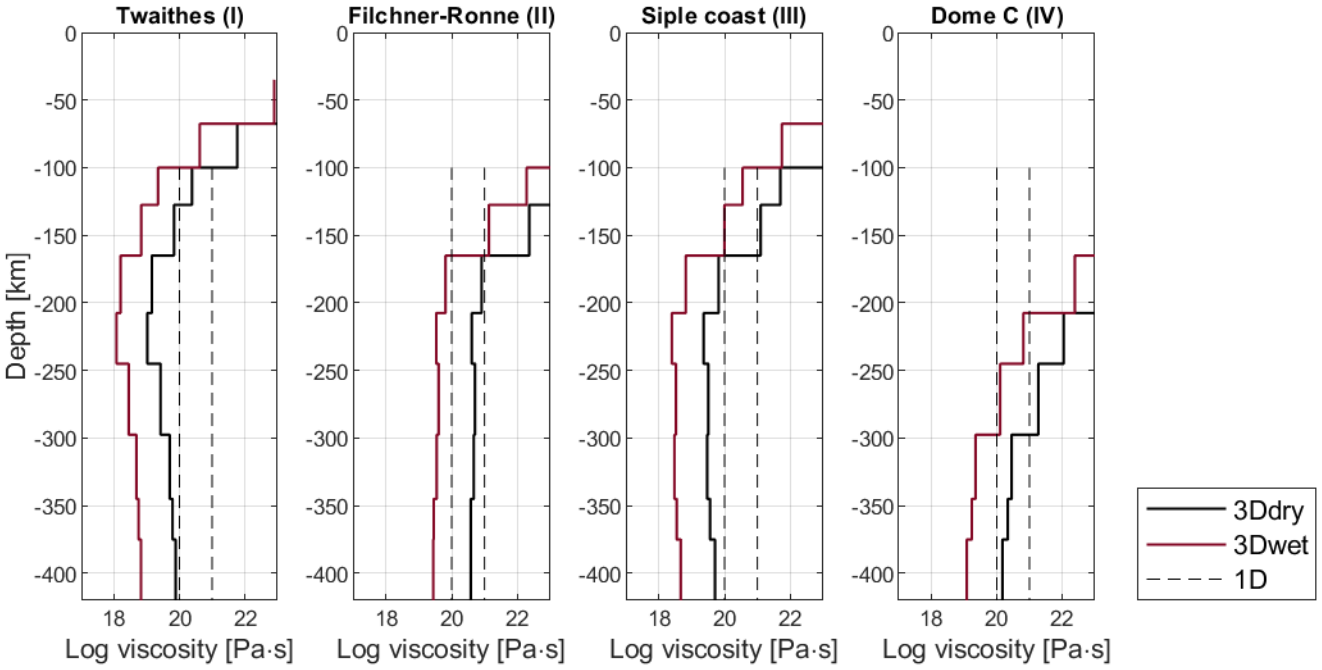

Figure S.4: Viscosity profile at 4 different locations; Thwaites glacier (-76.5531,-107.4472), Filchner-Ronne embayment (-78.8373,-62,5924), Siple coast (-79.2968,-149.0362), and Dome C (-75.1712,122.9052). The locations with corresponding numbers in the title are indicated in the map in Fig. 3a in the main manuscript. The viscosity is computed assuming a stress of 0.1 MPa.

45

Interpolation of bedrock deformation and ice loading

The total deformation computed by the GIA FE model that is used as input for ANICE, is defined on a regular grid of 0.25 by 0.25 degrees, whereas ANICE is defined on a polar stereographic equidistant grid of 40 km. Therefore, interpolation of the ANICE output, the change in ice thickness over the coupling time step, is needed to use the output of the ANICE as input for the GIA FE model. On the other hand, interpolation of the ANICE output is needed to use the output as input for the GIA FE model. For both interpolations we use Oblimap which is suitable for polar projections and takes into consideration conservation of mass (Reerink et al., 2016). The input for the GIA model is defined on a regular grid of 0.25 degrees latitude and longitude. For interpolation from the fine grid size of input of the GIA FE model to a somewhat coarser grid size of ANICE, the so-called radius method is used as this is computationally fast and provides an accurate result (Reerink et al., 2016). All fine grid points within a radius of the order of half the coarse grid size are included by a Shepard distance-weighted averaging interpolation method to obtain a representative value for this coarse grid point (Shepard, 1968). The quadrant method is used for gridding from a coarser ANICE grid to a somewhat finer input grid of the GIA FE model (Reerink et al., 2016). The region around the grid point of the fine grid is divided in four quadrants. For each quadrant, the closest grid point in the coarse grid is selected and shepard distance-weighted averaging is applied to these coarse grid points using a Shepard's power parameter of 2 (Shepard, 1968). A lower parameter would result in a smoother output but also less detailed. Furthermore, the ice thickness is linearly interpolated from the regular input grid of 0.25 degrees latitude by 0.25 degrees longitude to the irregular grid of the actual GIA FE sphere.

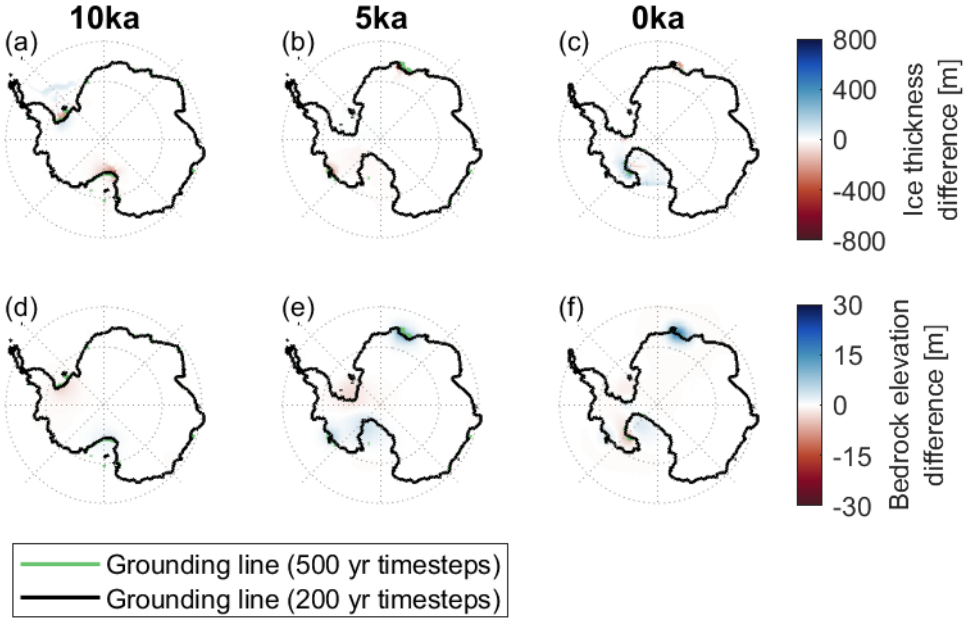

Figure S.5: Two tests were performed using the 1D21 rheology to test the sensitivity of the model to the length of the coupling time step. Panels a-c show the difference in ice thickness of the 200 yr time step simulation minus the ice thickness of the 500 yr time step simulation at three different moments in time, 10 ka, 5 ka and present day respectively. Panels d-f show the difference in bedrock elevation of the 200 yr time step simulation minus the bedrock elevation of the 500 yr time step simulation at three different moments in time, 10 ka, 5 ka and present day respectively.

Table S.1: Two simulations were performed to test the sensitivity of the model to the length of the couping time step. The length of the timestep of the test with 500 yr time steps is shown in table 2 in the main text. Here, we show the time step size of the test with 200 yr time steps during the deglaciation phase.

Period [ka]	Time step size [kyr]
120 – 20	5
20 – 15	0.5
15 – 5	0.2
5 – 1	0.5
1 - 0	0.2

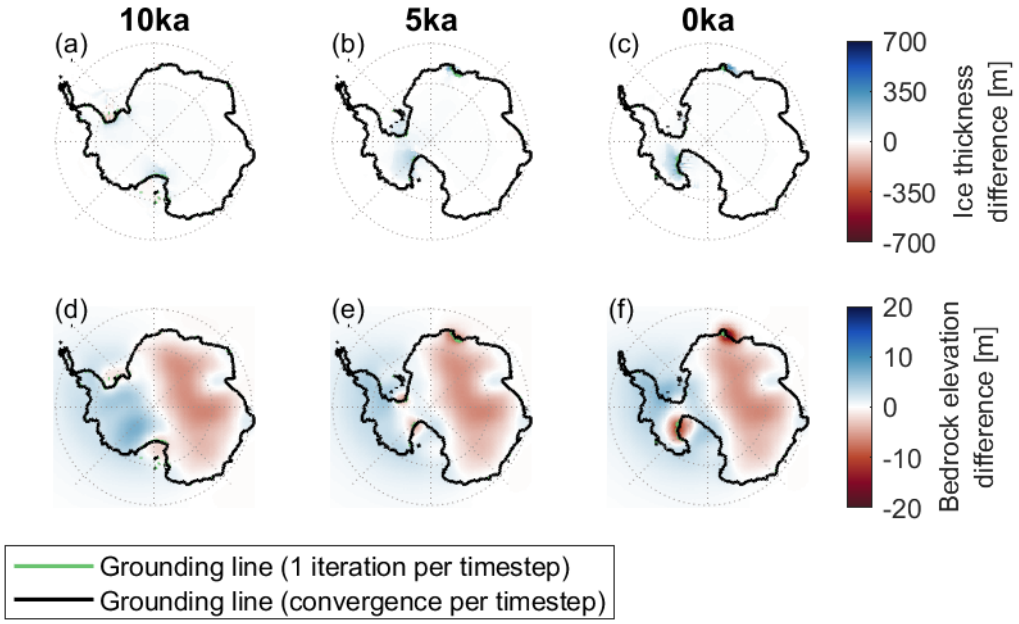

Figure S.6: The results of two simulations are shown using the 1D21 rheology. One test where the iterations are performed per coupling time step until the convergence threshold of 3mm/yr has been met, and one test where only one iteration is performed. Panels a-c show the difference in ice thickness of the convergence simulation minus the ice thickness of the 1 iteration simulation at three different moments in time, 10 ka, 5 ka and present day respectively. Panels d-f show the difference in bedrock elevation of the convergence simulation minus the bedrock elevation of the 1 iteration simulation at three different moments in time, 10 ka, 5 ka and present day respectively.

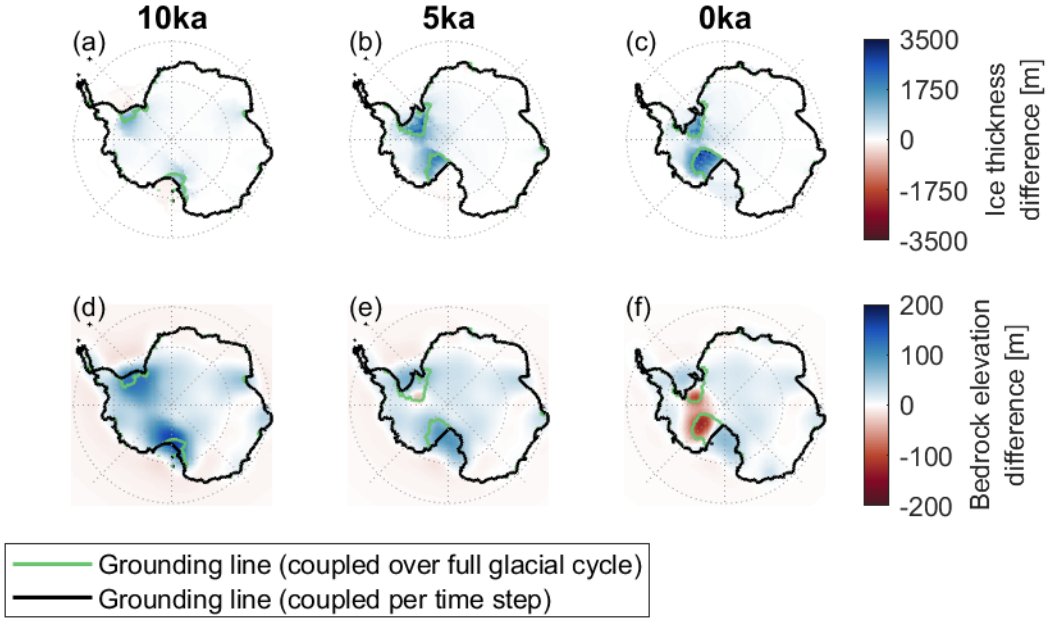

Figure S.7: The results of two simulations for the 1D21 rheology. One test where only one iteration is performed per coupling time step and one test where there is no iteration performed per coupling time step. Panels a-c show the difference in ice thickness of the convergence simulation minus the ice thickness of the 1 iteration simulation at three different moments in time, 10 ka, 5 ka and present day respectively. Panels d-f show the difference in bedrock elevation of the convergence simulation minus the bedrock elevation of the 1 iteration simulation at three different moments in time, 10 ka, 5 ka and present day respectively.

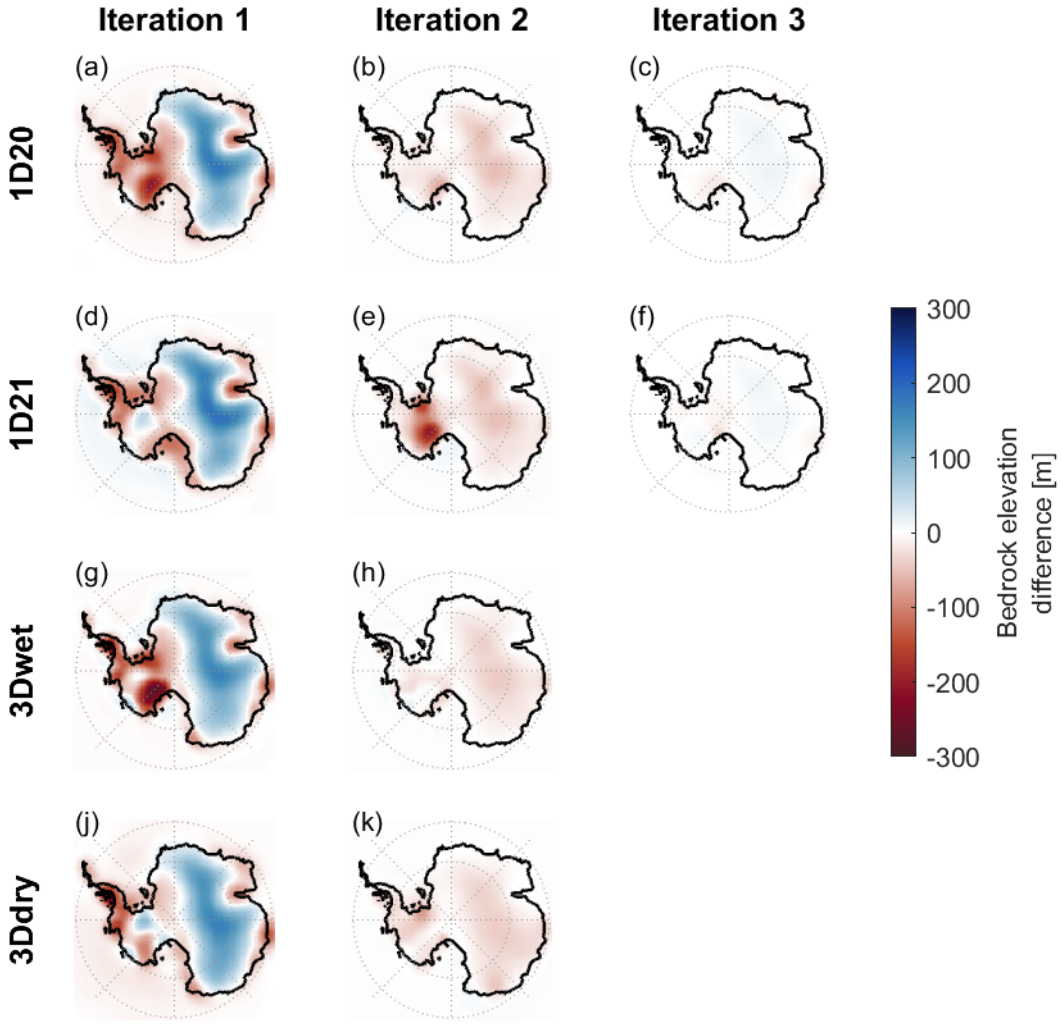

Figure S.8: Difference in bedrock elevation between topography at the final time step of the simulation and the observed present-day topography for the first three iterations over the glacial cycle using Earth structures 1D20 and 1D21, and two iterations using 3Dwet and 3Ddry.

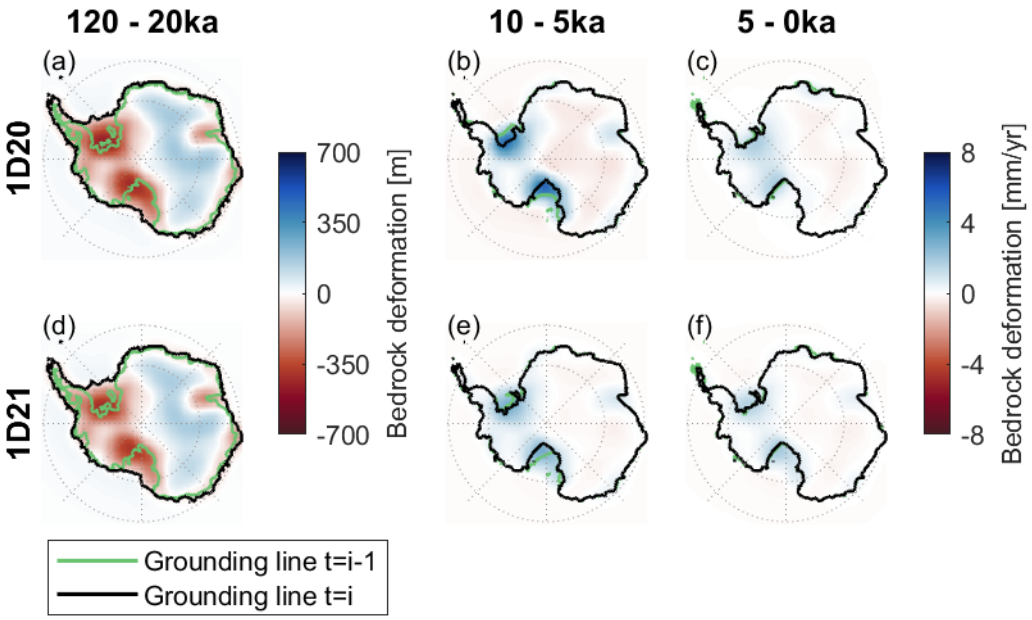

Figure S.9: Uplift over the glaciation phase and uplift rates between 10ka and present day for the 1D20 (panels a-c) and the 1D21 rheologies (panels d-f). The green grounding line shows the grounding line position at the beginning of the period over which the uplift is computed, and the black grounding line shows the position at the end of the period.

105